Paper:

Identification, Monitoring, and Assessment of an Active Landslide in Tavan-Hauthao, Sapa, Laocai, Vietnam – A Multidisciplinary Approach

Manh Duc Nguyen[*1,†], **Nguyen Van Thang**[*2], **Akihiko Wakai**[*2], **Go Sato**[*3], **Jessada Karnjana**[*4], **Hoang Viet Hung**[*5], **Lanh Si Ho**[*6,*7], **Indra Prakash**[*8], **Hoc Tran Quang**[*9], and **Binh Thai Pham**[*6]

[*1]University of Transport and Communications
No.3 Cau Giay Street, Lang Thuong Ward, Dong Da District, Hanoi, Vietnam
[†]Corresponding author, E-mail: nguyenducmanh@utc.edu.vn
[*2]Gunma University, Gunma, Japan
[*3]Teikyo Heisei University, Tokyo, Japan
[*4]National Electronics and Computer Technology Center, Pathum Thani, Thailand
[*5]Thuyloi University, Hanoi, Vietnam
[*6]University of Transport Technology, Hanoi, Vietnam
[*7]Civil and Environmental Engineering Program, Graduate School of Advanced Science and Engineering, Hiroshima University, Hiroshima, Japan
[*8]Geological Survey of India, Gandhinagar, India
[*9]University of Transport and Communications, Hanoi, Vietnam
[Received November 30, 2020; accepted March 29, 2021]

The active landslide located in the Tavan-Hauthao, Sapa district, Laocai province, Vietnam was investigated using geophysical methods (2D Electrical Resistivity and Tomography), geotechnical investigations, and a ground survey to assess the geologic condition of the sliding block and surrounding ground. Landslide displacement was measured using 15 surface monitoring points. Numerical modeling was done to assess the behavior of an active landslide. This multidisciplinary approach helped in interpreting landslide stratigraphy, geotechnical characteristics of the sliding groundmass, depth, and nature of the sliding plane. The surface area of the slide is approximately 1200 m^2. Studying this active landslide is important as it affects the road No. 152, which is an important road connecting the Sapa Ancient Rock Field. This study involved surface topographical survey, surface and sub-surface geological, and geotechnical investigations including Standard Penetration Test and Electrical Resistivity Tomography. Geologic and geotechnical data were used to characterize an active landslide block, which is composed of different soil layers underlaid by granitic rock. The surface electrical-resistivity measurements across the Sapa landslide resulted in inverted-resistivity sections with distinct resistivity contrasts that correlated well with the geology and geo-hydrology observed in boreholes.

Keywords: landslide, slip surface, resistivity inversion, numerical model, surface moving monitoring

1. Introduction

A landslide is the movement of a mass of rock, earth, or debris down a slope. Landslides are natural, complex phenomena whose study requires a multidisciplinary approach including geological, geotechnical, and geophysical investigations and meteorological data analyses [1]. Landslides are also caused by anthropogenic activities, such as excavation of slopes for construction of civil engineering structures (e.g., roads, dams, powerhouses, buildings). One of the main triggering factors for a landslide is rainfall and occasionally seismic activity. Landslides may cause significant loss of life and destruction of infrastructure and communication systems. Topography, geology, meteorology, and other geo-environmental factors play important roles in the occurrence of landslides. Understanding the mechanism and nature (type) of landslides [2] are important for landslide risk management and designing stable slopes.

Landslide identification plays an important role in landslide risk assessment and management [3]. With the advent of remote sensing technology, landslides can be identified through visual interpretation of both remote sensing images and topographic surfaces [4]. There are many methods and techniques for identifying large-scale landslide blocks, such as: locating the critical slip surface (CSS) and determining the factor of safety (FS), which are two key tasks in slope stability analysis. Traditional limit equilibrium methods (LEMs), such as the Bishop [5], Morgenstern and Price [6], and Spencer [7] methods are still the dominant slope stability analysis methods and have remained essentially unchanged for decades [8].

Fig. 1. Study location (Source: WorldAtlas and Google Maps).

Based on the limit equilibrium technique the CSS in a slope stability analysis is found using the stress acceptability criterion [9]. Other methods include an extension of Spencer's circular model for stability analysis of landslides with multi-circular slip surfaces [10]; a potential slip mass stability analysis using a modified slip surface stress method [11], and a landslide analysis for identification and extraction of geomorphological features of landslides using slope units [12]. Two independent models, an expert-based or heuristic and a statistical model (logistic regression), were developed to assess the landslide hazard [13]. Recently machine learning methods were used in landslide studies [14–16]. However, there is no substitute for field data when inputting and validating the models.

In the present study, one of the prominent active landslide located in Tavan-Hauthao commune, Sapa town, Laocai province was selected for the detailed geotechnical and geophysical (Electrical Resistivity Tomography) investigations. Surface movement monitoring and numerical model analysis were carried out to identify plain failure and to evaluate its characteristics for the treatment and management of the landslide affected area (**Fig. 1**). This landslide has been active since 2010 and is affecting the alignment of inter-provincial important road No. 152 over a 50 m length (from km7 + 550 to km7 + 600), which is located on a sliding groundmass (block). This road connects Sapa Ancient Rock Field, which is of national and international importance. Habitation surrounding the sliding block also has been affected in the Tavan-Hauthao area. Road No. 152 passes through the terraced rice paddies of Muong Hoa Valley, approximately 12 km southeast of Sapa town in the Tavan-Hauthao commune. This area (about 8 km^2) of old carved stone in Sapa is also a UNESCO world heritage site. In view of the importance of this area, systematic geotechnical and geophysical investigations were carried out for landslide treatment and management. There is an urgent need to stabilize the sliding block and to construct a safe road to maintain continuous traffic to national and international historical rock monuments.

The study included a surface topographical survey (surface moving monitoring from 2018 to 2020), surface and sub-surface geological and geotechnical investigations, including Standard Penetration Test (SPT), numerical model analysis by Plaxis software, and Electrical Resistivity Tomography (ERT) to identify the type of landslide, in addition to the characteristics and geotechnical engineering properties of the sliding block (groundmass).

2. Study Area Description

The Sapa district (Lat.: 22°07′04″, Long.: 22°28′46″) of Laocai province is located to the east of the Hoang Lien Son mountain range. The elevation of Sapa town ranges from 1,200 m to 1,800 m. The topography of the area is hilly with mountain peaks and valleys. Hill Slopes in the area vary generally from 35°–40°. Sapa area has a cold temperate climate with two main seasons: rainy (May to October) and winter with little rain (November to April). The annual average temperature is 15.4°C and the average annual rainfall is approximately 2,762 mm in this area.

2.1. Geological Setting

The study area has a complex geological structure associated with tectonic faults mostly aligned in the Northwest–Southeast direction [17]. Geology of the area is comprised of various lithological units ranging from the Proterozoic Era to Quaternary Period. These rock formations include the Da Dinh formation (NP_3-$\varepsilon_1 đđ$) of the Proterozoic Era including marble rocks, dolomite rocks, marble with thick layers of tremolite; the Cha Pa formation (NPcp), which is comprised of sericite quartz schist and marble; the Cam Duong formation from the Cambrian–Ordovician Period, which includes a sub-formation ($\varepsilon_1 cd_1$) consisting mainly of conglomerate, gritstone, shale, lime, and apatite; the Po Sen complex formation ($\delta\gamma PZ_1 ps$), which is comprised of diorite, granodiorite, and granite; the Ban Nguon formation ($D_1 bn$) of the Siluric–Devonian Period, which includes shale and sandstone containing lime; and the Ban Pap formation ($D_{1\text{-}2} bp$), which contains thin-layered limestone and clay-limestone. The Ye Yen Sun complex formation (γEys) is comprised of granite and alkaline grano-syenite, which is the youngest rock formation of the Paleogene Period, followed by Quaternary (dp) sediments comprised mainly of cobbles, gravel, sand, and clay with an average thickness of 1 to 5 m (maximum thickness 10 m). The Muong Hoa Valley, which is 1000 m at its lowest altitude, is the result of endogenous processes, such as tectonic, neo-tectonics, and recent geodynamic activities.

2.2. History of the Landslide

The landslide under investigation is located in the Tavan-Hauthao commune, within the conservation area of the Antique Engraved Rocks area in the Sapa district. This landslide is affecting provincial road No. 152 because it passes through the center of the landslide. The head of the landslide is on the slope of the Ham Rong

Mountain and the toe is located on the valley slope of the Muong Hoa stream (**Fig. 1**).

Since 2010, a section of provincial road No. 152, covering approximately 50 m length from km7 + 550 to km7 + 600, has been observed moving in both vertical and horizontal directions. In 2017, the largest recorded vertical displacement of the road surface was approximately 1.0 m and the largest recorded horizontal displacement (curved roadbed) was more than 2 m. From November 2018 to July 2019, part of the road was subsiding, which resulted in a vertical displacement of more than 1.5 m. From November 2019 to August 2020, it was recorded to be more than 2 m. The stability of the residential cluster adjacent to road No. 152 and on the surrounding groundmass of the sliding block is in danger.

3. Geotechnical Investigation

The layout of the exploratory drilling carried out in the study area to determine stratigraphy and geotechnical properties of the sliding groundmass (block) is presented in **Fig. 2**. Soil samples were analyzed in the laboratory to determine the in-depth engineering properties of the sliding block and shear parameters using the SPT. Results of the exploratory drilling (boreholes LKS1, LKS2, LKS3, LKS4) and SPT are summarized below:

1. Soil layer No. 1: Clay mixed with crushed gravel, crushed lump gravel with a reddish-brown, dark gray, gray color in a semi-solid state, with an average thickness of 4.7 m, SPT value ranging from 15 to 18, average *N*-value of SPT is 16.
2. Soil layer No. 2: Clay mixed with crushed gravel, crushed lump gravel with a yellowish brown, red-brown, dark gray color. Clay is a soft plastic type with an average layer thickness of 3.4 m and SPT value ranging from 4 to 8, average *N*-value of SPT is 5.
3. Soil layer No. 3: Clay mixed with crushed gravel, crushed lump gravel with a red-brown, dark gray, brown-gray color. The layer is in a semi-solid state, with a thickness ranging from 7 m to 18.5 m with SPT value ranging from 15 to 32, average *N*-value of SPT is 17.
4. Soil layer No. 4: crushed gravel, crushed lump gravel mixed with white clay, brown-gray clay (products of weathered rocks). This layer is in a solid plastic to semi-solid state. Average layer thickness is 12.5 m, SPT values ranging from 8 to 27. Average *N*-value is 17.
5. Sub rock layer No. 5a: This layer includes gray color moderate to highly jointed granite rock with cracks, Total Core Recovery (TCR) is 10–20%, and Rock Quality Designation (RQD) is 5–10%. Average thickness of layer is 3.5 m and compressive strength < 70 MPa.
6. Sub rock layer No. 5b is located below layer No. 5a. This layer mainly consists of white and white gray slightly to moderately jointed granite rock, TCR is 30–40% and RQD is 20–30%.

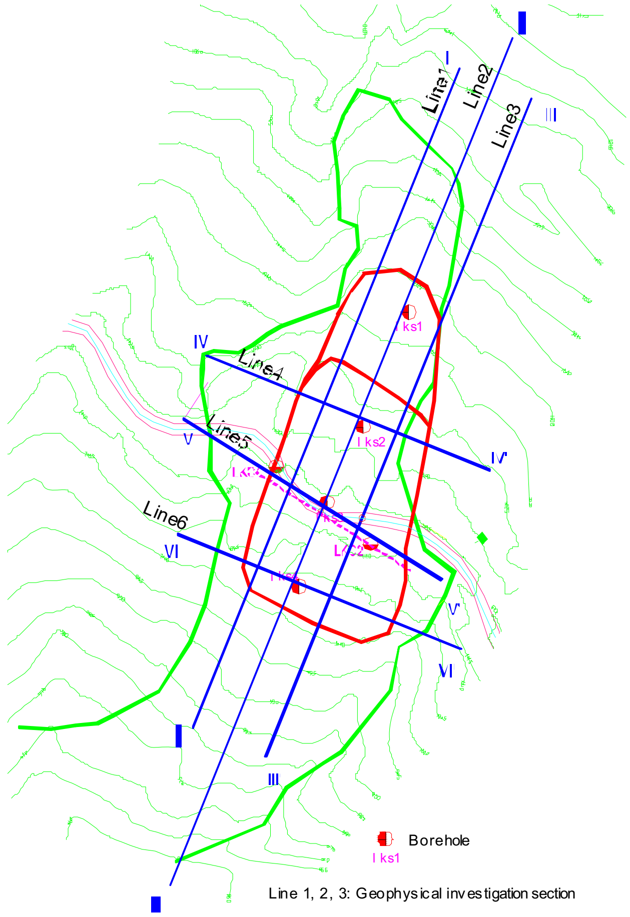

Fig. 2. Layout of geotechnical survey boring holes and section lines of deep electrode resistivity measurement [18].

The thickness of the soil layers of the sliding block varies from 12.5 m to 40.5 m. These soil layers contain coarse grain content (d < 0.5 mm) more than 11%. *N*-values vary from 5 to 27. Generally, *N*-value increases with the depth. These soil layers that form sliding blocks are underlaid by jointed granitic rocks (RQD: 5 to 30%) just below the sliding plain.

4. Electrical Resistivity Tomography (ERT)

The technique of 2D ERT has been successful for imaging many different types of landslides in order to detect slide planes, lithologic interfaces, and moisture regimes [19]. The surface measurements were carried out in two arrays, perpendicular and parallel, to the slope direction.

The layout of the 2D ERT investigations carried out in the sliding area is presented in **Fig. 2** along with the layout of the Geotechnical Survey. Geophysical investigations were conducted along six sections, at measuring points 5 m apart (**Figs. 3–5**). The 2D Imager software was

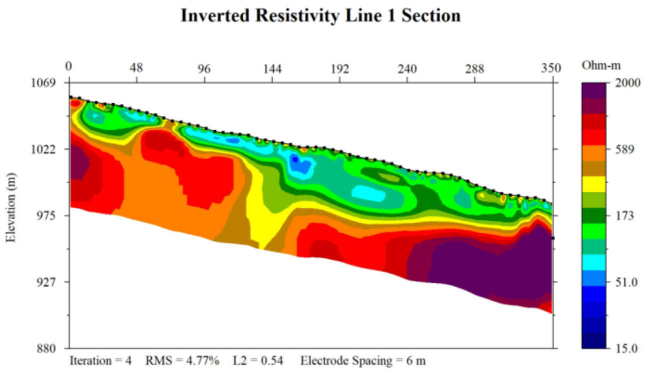

Fig. 3. Resistivity Imaging of section Line 1 [18].

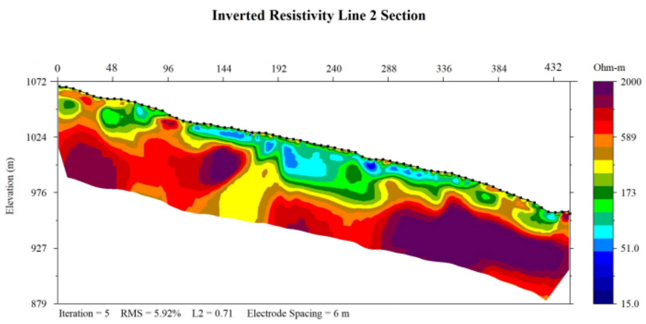

Fig. 4. Resistivity Imaging of section Line 2 [18].

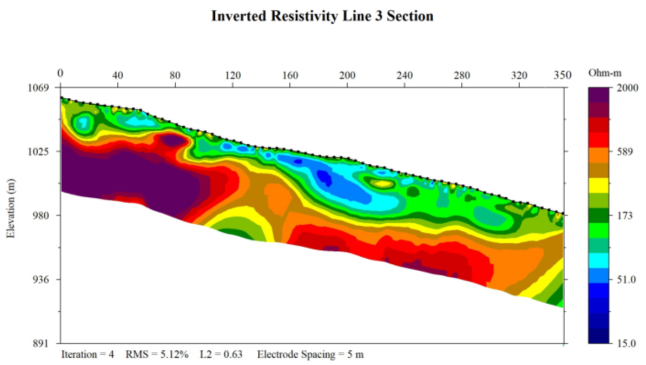

Fig. 5. Resistivity Imaging of section Line 3 [18].

used for analyzing and interpreting geophysical data. For this task, we have used Earth Imager 2D software to analyze the Resistivity Images for extracting the geological-geophysical profile [20].

5. Resistivity Results

Geophysical ERT data was collated with geotechnical data for delineating different litholayers considering geology, engineering properties, moisture content, electrical resistivity, and SPT values. **Figs. 6**, **7**, and **8** represent the analyzed results of geological and geophysical profiles along section Lines 1, 2, and 3, respectively.

The ERT study (**Figs. 6–8**) correlated with the geophysical and geological/geotechnical data. The continuous transformation of horizontal and vertical resistivity values for all measurement lines using the 2D Multi-Electrode method (**Figs. 3–5**) demonstrates that the stratigraphy and physical properties of the soil and rock layers vary laterally as well as in-depth for the sliding groundmass (block) under study.

Figures 3–5 indicate low resistivity anomaly zones ($\rho = 15/60\ \Omega$m) represented by a dark blue color in these sections. These low resistivity anomaly zones are weak lithology zones comprised of poorly compacted and low-strength soil/rock, which may also contain groundwater. Based on the abnormal resistivity zone at depth, a potential sliding surface was identified as a sliding mass (**Figs. 6–8**). A seepage of groundwater was observed at the toe of the sliding blocks, which confirmed the resistivity survey results.

In addition, at the middle of Line 1, Line 2, and Line 3, anomaly zones with relatively different (relatively low) resistivities were detected in the bedrock. The sudden decline in resistivity $\rho = 300/500\ \Omega$m in the rock zone from $\rho = 1000/2000\ \Omega$m indicates the presence of jointed weathered rocks.

6. Numerical Model Analysis of the Landslide

The numerical model analysis was conducted using Plaxis 2D v20 software. The soil parameters used in this study are results of a geological-geophysical profile, geotechnical investigation results of contiguous constructions, and back analyzed data. Geological layers 1, 2, 3, and 4 used the Morh-Coulomb soil material model (MC), and the stone layer 5a and 5b used the bedrock model (BR), as shown in **Table 1**.

A sequence of installing phases in Plaxis 2D included the following phases: Phase 1, Initial phase (the initial situation consisting of the intact hill side and a phreatic level representing typical summer conditions). The geometry has a non-horizontal soil layering, hence the K0-procedure could not be used, therefore, we set the calculation type to gravity loading. In water conditions mode, we set a phreatic level; Phase 2, factor of safety (FOS) of the hillside in the summer conditions (before the condition is started the FOS is determined by the initial situation. This calculation phase is safety and we accepted all default settings); Phase 3, Winter conditions (the increase in water level should occur after the process due to specific rainy weather conditions locally and not after determination of the factor of safety for this situation). Therefore, we went with the staged construction definition and from there to the water conditions mode and set a new phreatic line; Phase 4, FOS of the hillside in winter conditions (the same setup and analysis as phase 2). Parameters used in the model included unit weight, Cohesion, Friction angle, which are results from the geotechnical investigation. The model used in the three analytical sections is shown in **Figs. 9–11**. The results of the dis-

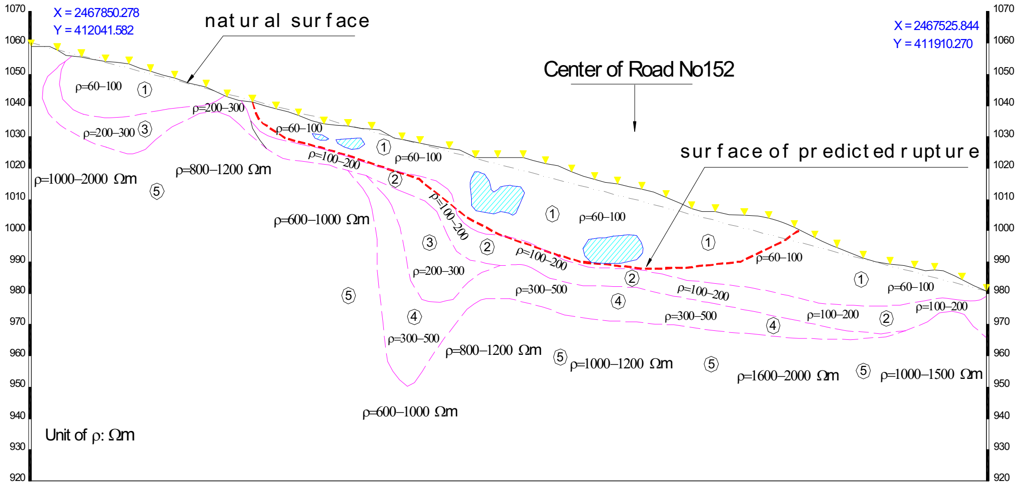

Fig. 6. Geological-geophysical profile of Line 1.

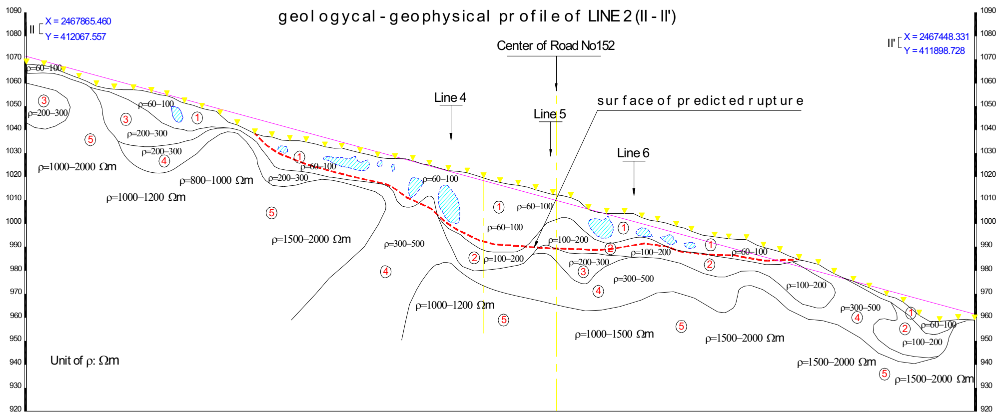

Fig. 7. Geological-geophysical profile of Line 2.

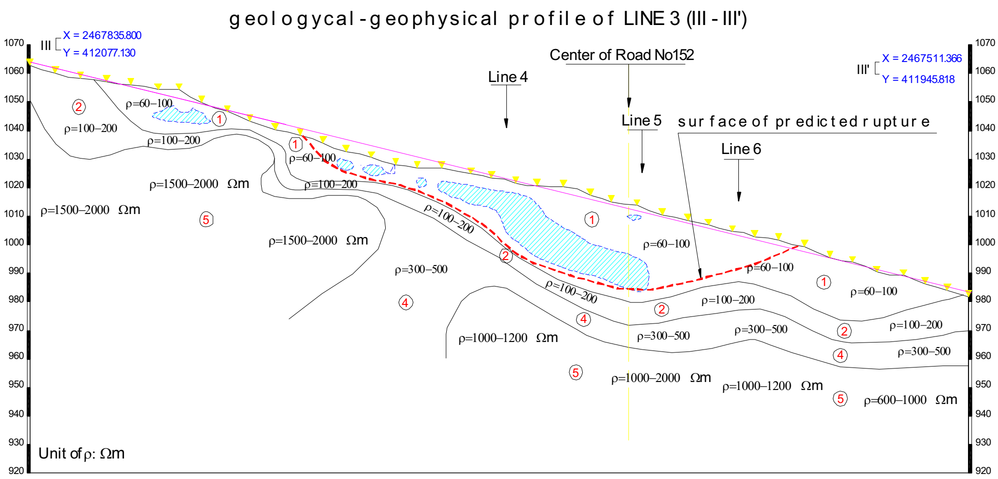

Fig. 8. Geological-geophysical profile of Line 3.

Table 1. Soil parameters used to analyze the numerical model.

Geological layers	Material model	Unit weight [kN/m^3]	Phi [°]	Cohesion [kPa]
Layer 1	MC	19.00	12.00	15.00
Layer 2	MC	17.80	13.65	15.03
Layer 3	MC	17.89	17.55	23.10
Layer 4	MC	18.34	18.02	19.43
Layer 5a	BR	–	–	–
Layer 5b	BR	–	–	–

*MC: Morh-Coulomb; BR: Bedrock.

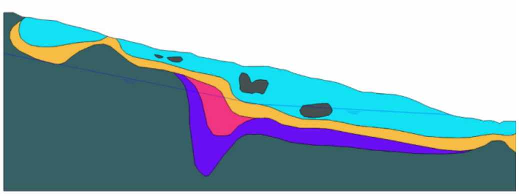

Fig. 9. Modeling Line 1.

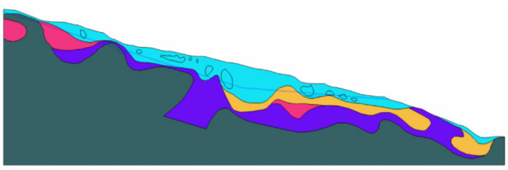

Fig. 10. Modeling Line 2.

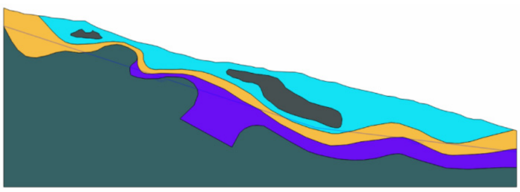

Fig. 11. Modeling Line 3.

placement analysis are shown in **Figs. 12–16**.

The results of a numerical model analysis (**Figs. 12–16**) showed that the predictive slip surface and displacements, which are suitable to the 2D resistivity inversion of ERT data-anomalies zone of the 2D electrical imaging result, and weathered cover, as well as the results of the geotechnical-geophysical analysis (**Figs. 3–8**).

7. Monitoring and Validation of the Data

Shifting or displacement of a point or building from its original position with time can be measured by determining the coordinates and elevation of that point with instruments. For 2 or more measurement cycles, the dis-

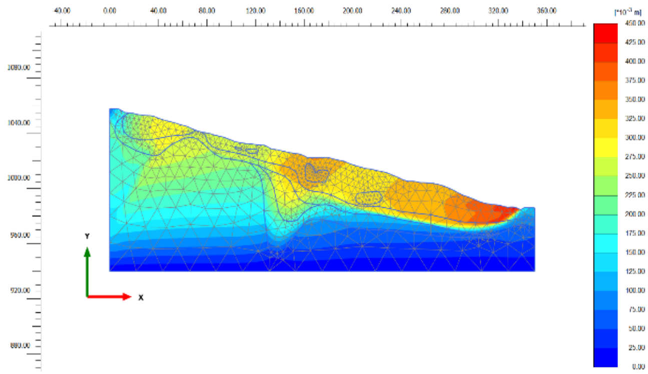

Fig. 12. Predictive displacements at Line 1.

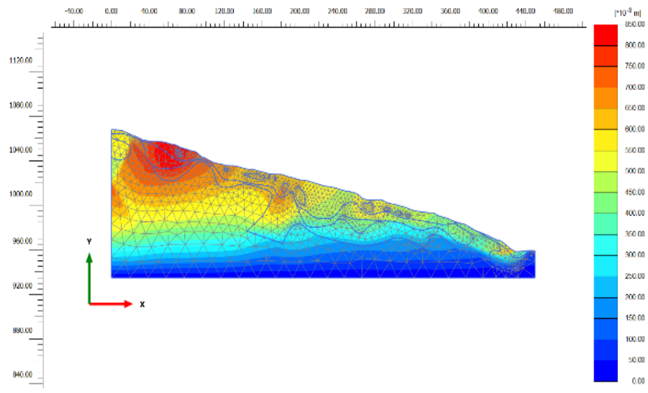

Fig. 13. Predictive displacements at Line 2.

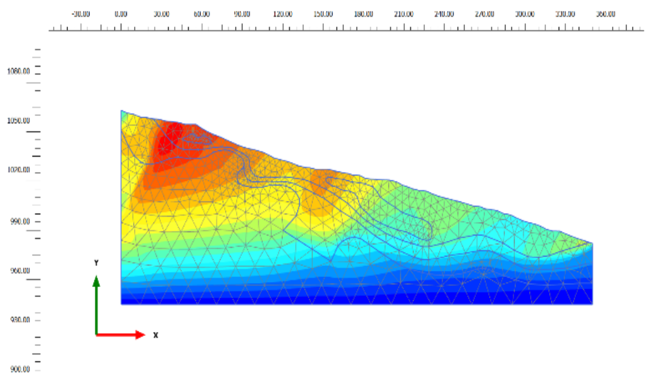

Fig. 14. Predictive displacements at Line 3.

placement value was calculated according to the formula:

- The horizontal displacement:

$$Q_{12} = \sqrt{Q_X^2 + Q_Y^2}, \quad \dots \dots \dots \dots \quad (1)$$

- The vertical displacement (heaven, settlement):

$$S_{12} = H_i^2 - H_i^1, \quad \dots \dots \dots \dots \quad (2)$$

where: $Q_X = X_i^{(2)} - X_i^{(1)}$, $Q_Y = Y_i^{(2)} - Y_i^{(1)}$; $X_i^{(1)}$, $Y_i^{(1)}$, $H_i^{(1)}$, $X_i^{(2)}$, $Y_i^{(2)}$, $H_i^{(2)}$ are the coordinate values and elevation point of cycles (1) and (2).

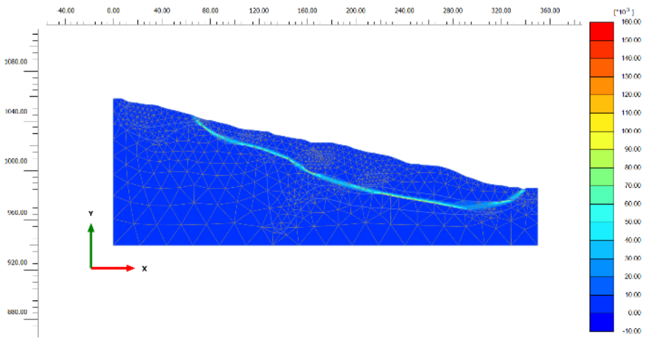

Fig. 15. Predictive slip surface of landslide at Line 1.

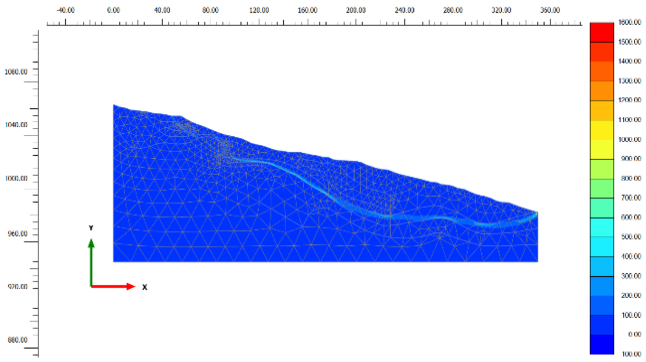

Fig. 16. Predictive slip surface of landslide at Line 3.

7.1. Establishing a System of Measuring Points in the Sliding Area of Hau Thao

In order to conduct monitoring shifting (displacement) of sliding blocks, the system of landmarks, including benchmarks and monitoring landmarks, were designed and established. The benchmarks were selected outside of the risk area (in a stable area) of the landslide to serve as a basis for monitoring the relative displacement on the surface of the sliding block. The monitoring landmarks were established at locations where surface manifestations of the sliding movement were observed, such as cracks, upheaval, and deformation of linear features (e.g., roads, tilting of trees).

These benchmarks and monitoring landmarks were constructed in accordance with the technical standards of Vietnam (TCVN 9360; TCVN 9399, 2012). Considering the dimension of the sliding block in the Tavan-Hauthao area, three benchmarks (MC1, MC2, MC3) and 15 monitoring landmarks (QT1, QT2, ..., QT15) were constructed (**Fig. 17**).

7.2. Monitoring Results of Surface Displacement of the Landslide Block

The movement of the sliding block in the Tavan-Hauthao area was assessed by measuring the change of coordinates (horizontal displacement) and altitude (vertical displacement, subsidence) of observation landmarks in relation to the benchmark by time. An electronic to-

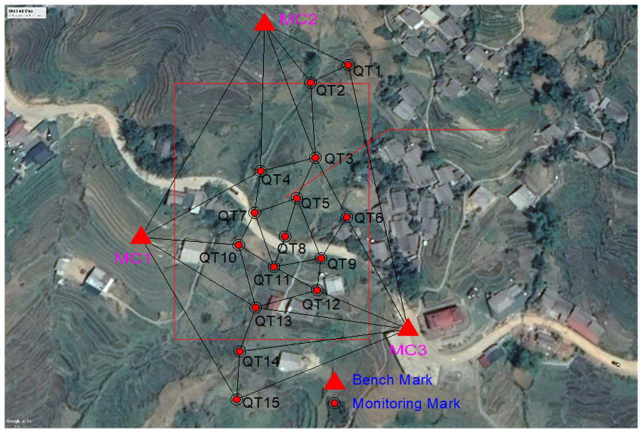

Fig. 17. Location of benchmarks and monitoring landmarks set in the Tavan-Hauthao sliding block.

tal station and high-precision GPS were used to determine the coordinates of benchmarks and monitoring landmarks. The devices used Trimble R8 devices with an accuracy of 3 mm + 0.5 ppm RMS in the horizontal direction, and 5 mm + 0.5 ppm RMS in the vertical direction. The altitudes of monitoring landmarks were determined using a leveling machine with high precision, with a measurement error of 2 mm for measuring a round trip of 1 km in length.

Monitoring work was conducted for 10 measurement cycles, from April 2018 to August 2020. The displacement on the surface of the sliding groundmass was determined by measuring the change of coordinates X, Y, and H (altitude) of the monitoring landmarks in 6 measurement cycles. The shifting (displacement) parameters were calculated using formulas (1) and (2) based on the measured values of coordinates and elevations. The results of the changes obtained by the instruments for all of the monitoring points are shown in **Tables 2** and **3** and **Figs. 18** and **19**.

Analysis of the instrument's data (**Tables 2** and **3** and **Figs. 18** and **19**) indicated that all of the monitoring points located on the sliding mass moved differentially in different magnitudes relative to each other during each measurement cycle. Monitoring points QT3, QT5, QT8, QT11, and QT13 located at the central part of the sliding block surface showed relatively large displacement values for all measurement cycles. The total value of the horizontal displacement of monitoring landmarks was approximately 0.54 m. The largest horizontal shift (displacement) of 1.6 m and a vertical shift of 0.71 m were observed at the QT13 landmark.

The surface vertical displacement of the sliding block was recorded for all 15 monitoring points during 28 months of observations (from April 2018 to August 2020) for 10 measurement cycles. The vertical displacement of monitoring landmarks varied and had different values between measurement cycles that clearly showed an increasing trend for vertical movement of sliding groundmass down to the toe of the slide (**Figs. 18**

Table 2. The horizontal displacement values of monitoring points that cross the landslide for 10 cycles.

Cycle	The horizontal displacement values of monitoring points [m]								
	QT1	QT2	QT3	QT5	QT8	QT11	QT13	QT14	QT15
Q2-1	0.011	0.007	0.006	0.008	0.005	0.016	0.029	0.004	0.008
Q3-1	0.009	0.009	0.063	0.101	0.131	0.098	0.213	0.003	0.008
Q4-1	0.055	0.026	0.126	0.146	0.259	0.179	0.398	0.034	0.032
Q5-1	0.020	0.009	0.129	0.168	0.298	0.215	0.446	0.019	0.011
Q6-1	0.016	0.014	0.133	0.184	0.318	0.234	0.472	0.030	0.002
Q7-1	0.006	0.011	0.196	0.276	0.511	0.380	0.664	0.028	0.034
Q8-1	0.009	0.012	0.296	0.418	0.717	0.526	1.032	0.030	0.080
Q9-1	0.012	0.015	0.364	0.418	0.868	0.647	1.287	0.030	0.119
Q10-1	0.007	0.012	0.457	0.671	1.091	0.814	1.613	0.030	0.145

Table 3. The vertical displacement values of monitoring points that cross the vertical line for 10 cycles.

Cycle	The vertical displacement values of monitoring points [m]								
	QT1	QT2	QT3	QT5	QT8	QT11	QT13	QT14	QT15
S2-1	0.008	0.010	0.007	0.004	0.000	0.010	0.009	0.001	0.003
S3-1	0.047	0.031	0.013	0.001	0.023	0.050	0.120	0.003	0.049
S4-1	0.026	0.010	0.014	0.031	0.047	0.073	0.169	0.008	0.008
S5-1	0.023	0.002	0.014	0.030	0.051	0.086	0.194	0.002	0.004
S6-1	0.021	0.007	0.013	0.029	0.054	0.098	0.220	0.003	0.001
S7-1	0.023	0.005	0.019	0.044	0.100	0.115	0.391	0.009	0.021
S8-1	0.022	0.001	0.038	0.103	0.145	0.159	0.444	0.002	0.055
S9-1	0.024	0.004	0.044	0.108	0.198	0.234	0.533	0.004	0.060
S10-1	0.026	0.015	0.053	0.147	0.234	0.309	0.712	0.007	0.069

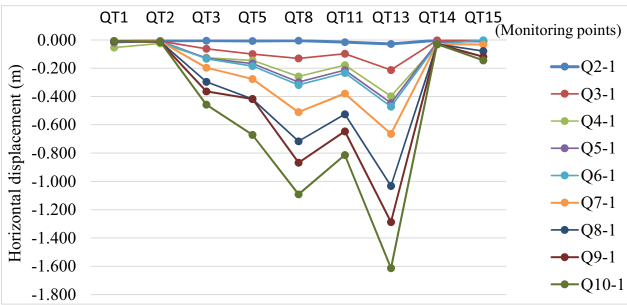

Fig. 18. The horizontal displacement of monitoring landmarks after 10 measurement cycles.

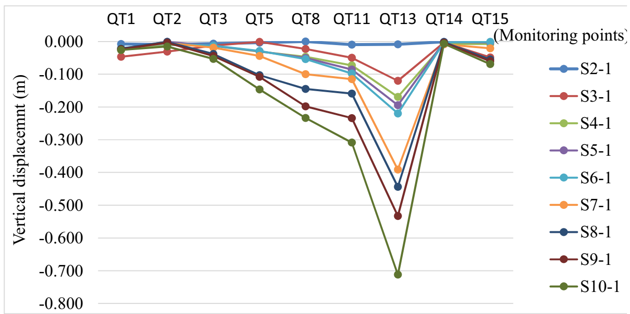

Fig. 19. Vertical displacement of monitoring points after 10 measurement cycles.

and **19**). The monitoring landmarks QT3, QT5, QT8, QT11, and QT13 on the sliding block had large vertical and horizontal shift/movement values, which is consistent with the actual observation of surface manifestations over time from 2010 to the present (2021).

During the rainy season (June to September of each year), which corresponds to the second through fourth cycle of measurement, the movement on the surface of the sliding block greatly increases (2–3 times higher) in comparison to the dry season.

The results of monitoring the surface of the sliding block in Tavan-Hauthao indicated that the groundmass is progressively sliding on both sides (including slopes at upper and lower side) of road No. 152.

Sub-surface data obtained from the geophysical survey has been validated using exploratory drilling data. Vertical and horizontal displacements of the groundmass have been progressively measured (horizontal and vertical distances with movement directions) in the field using precision survey equipment.

8. Discussion

Geophysical investigations, specifically electrical resistivity, provide an overall view of the subsurface that can be used to supplement drilling and be correlated with soil properties.

Progressive observations of the alignment of provincial road No. 152 from 2010 until the present (2021)

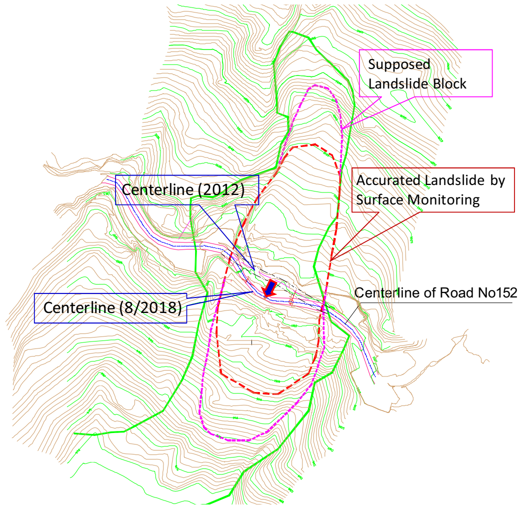

Fig. 20. Sketch of shifting of provincial road No. 152 over time and landslide area identified.

Fig. 21. Study of the sliding block in Tavan-Hauthao (July 2020).

indicate that the section of this road from km7 + 550 to km7 + 600, which passes through sliding groundmass, has been changing from a gentle arc to more curvilinear due to its location on an active slide. Convexity of the road is gradually increasing toward a downhill slope that is in the direction of the valley (**Fig. 20**). Average horizontal movement/shifting of the road section located at the central part of the curvature is 1–2 m/year and vertical movement/displacement is 0.6 to 1.2 m/year (at the road surface of No. 152).

Results of the surface and sub-surface geotechnical investigations confirmed that the deformation of road No. 152 is due to sliding of the groundmass on which it was constructed (**Fig. 20**).

Based on the geotechnical and geophysical investigations, and results of numerical model analysis, the potential slip surface of sliding blocks was identified (**Figs. 6**, **7**, **8**, **15**, and **16**)

Figures 20 and **21** show the sloping topography of the study area with a dip toward the river valley bottom. An erosional gulley along the western side of the slide was formed with time, which acts as a drainage and seepage path for saturating adjacent groundmass, including sliding soil block. The presence of anomalous weak zones was identified at depth from geotechnical investigations in conjunction with the ERT. These weak zones suggest that the groundmass has low shear strength and high permeability. A curvilinear sliding plane was identified through sub-surface exploration. Seepage of water through agriculture activity and rainwater appears to be the main cause of this landslide besides removal of toe support due to progressive erosion of the river valley slope. Initially, the landslide appears to have started as a translational type, but subsequently developed into a concave rupture plane in groundmass near the contact of soil and rock and formed as a mixed type rotational slide.

The extremely slow movement of surface soil layers on the slope is a result of climate-driven cyclical volume changes (wetting and drying). It is well known that volumetric expansion acts normal to the sloping ground surface while, during shrinkage, the material moves down vertically under gravity. The result is a net down slope movement, termed soil creep [21]. The rates of movement are extremely slow [22], but, over long periods of time, most steep slopes become mantled by slow movement. This cyclic phenomenon has nothing in common with the mechanistic meaning of the term "creep," but is used here as a long-established practice. The mechanism of "soil creep" related to such slides is described in detail by Varnes [2].

In the present case, the movement of a landslide is not simply a case of soil creep. It is a complex process associated with the subsurface flow of water along a slip plane and loading of the groundmass; and removal of toe support due to natural and anthropogenic factors.

9. Conclusions

Geologic and geotechnical data were used to characterize an active landslide block, which is composed of different soil layers underlaid by granite rock. The surface electrical-resistivity measurements across the Sapa landslide resulted in inverted-resistivity sections with distinct resistivity contrasts that correlated well with borehole stratigraphy, depth, and groundwater conditions. Low-resistivity zones were indicators of shear planes associated with weak permeable zones which are correlated with the failure surface of the landslide. The inverted-resistivity profiles confirmed the curve-planar and undulating nature of the failure surface as indicated by the geotechnical investigation.

There is a cluster of residential buildings around the landslide that need to be protected from foundation disturbances likely to be caused by further progressive movement of the sliding groundmass. Moreover, road No. 152 is an important connecting road for approaching national and international cultural heritage sites, including the Sapa Antique Engraved Rocks Area. Therefore, it is necessary to maintain adequate road traffic by ensuring smooth and safe traffic for the travelers visiting this tourist location. Due to the presence of residential clusters and heritage structures adjacent to and nearby the present sliding block, construction of a connecting road above the crown or below the toe of this active slide is not desirable as it would require significant ground excavation. Another alternative for ensuring long-term, safe communication is the construction of a large span reinforced concrete bridge that crosses over the landslide area or by constructing bridge piers within the sliding area with a foundation on a stable rock. However, a suitable design is required to withstand the dynamic pressure of the sliding groundmass on the bridge piers.

The Tavan-Hauthao landslide is moving slowly. Factors contributing to the landslide include moderate slope, weak sliding groundmass, and jointed bedrock, associated with residential development. The data collected and interpreted in this study provided a detailed analysis of one landslide, but it can be used in future landslide hazard studies that combine geotechnical and geophysical techniques to investigate active landslides. However, real-time monitoring of such active sliding blocks are needed for taking timely remedial measures to prevent collapses and destruction of infrastructures.

Acknowledgements

The authors are grateful to the Vietnam Ministry of Science and Technology for their support. This work was supported by NDT 67/e-Asia19.

References:

[1] E. A. Castellanos Abella and C. J. Van Westen, "Qualitative landslide susceptibility assessment by multicriteria analysis: A case study from San Antonio del Sur, Guantánamo, Cuba," Geomorphology, Vol.94, Nos.3-4, pp. 453-466, 2008.

[2] D. J. Varnes, "Slope movement types and processes," R. L. Schuster and R. J. Krizek (Eds.), "Landslides: Analysis and control (Special reports No.176)," pp. 11-33, Transportation Research Board, National Academy of Sciences, 1978.

[3] A. Manconi et al., "Brief Communication: Rapid mapping of landslide events: The 3 December 2013 Montescaglioso landslide, Italy," Natural Hazards and Earth System Sciences, Vol.14, No.7, pp. 1835-1841, 2014.

[4] W. C. Haneberg, W. F. Cole, and G. Kasali, "High-resolution lidar-based landslide hazard mapping and modeling, UCSF Parnassus Campus, San Francisco, USA," Bulletin of Engineering Geology and the Environment, Vol.68, No.2, pp. 263-276, 2009.

[5] A. W. Bishop, "The use of the Slip Circle in the Stability Analysis of Slopes," Géotechnique, Vol.5, No.1, pp. 7-17, 1955.

[6] N. R. Morgenstern and V. E. Price, "The analysis of the Stability of General Slip Surfaces," Géotechnique, Vol.15, No.1, pp. 79-93, 1965.

[7] E. Spencer, "A method of analysis of the Stability of Embankments Assuming Parallel Inter-Slice Forces," Géotechnique, Vol.17, No.1, pp. 11-26, 1967.

[8] D. V. Griffiths and P. A. Lane, "Slope stability analysis by finite elements," Géotechnique, Vol.49, No.3, pp. 387-403, 1999.

[9] S. K. Sarma and D. Tan, "Determination of critical slip surface in slope analysis," Géotechnique, Vol.56, No.8, pp. 539-550, 2006.

[10] Z. Fan et al., "Extension of Spencer's circular model to stability analysis of landslides with multicircular slip surfaces," Mathematical Problems in Engineering, Vol.2020, Article No.1298912, 2020.

[11] H. Zhang et al., "Modified slip surface stress method for potential slip mass stability analysis," KSCE J. of Civil Engineering, Vol.23, No.1, pp. 83-89, 2019.

[12] Y. Hua et al., "Dynamic development of landslide susceptibility based on slope unit and deep neural networks," Landslides, Vol.18, No.1, pp. 281-302, 2021.

[13] C. Jaedicke et al., "Identification of landslide hazard and risk 'hotspots' in Europe," Bulletin of Engineering Geology and the Environment, Vol.73, No.2, pp. 325-339, 2014.

[14] M. Sahana et al., "Rainfall induced landslide susceptibility mapping using novel hybrid soft computing methods based on multi-layer perceptron neural network classifier," Geocarto Int., doi: 10.1080/10106049.2020.1837262, 2020.

[15] B. T. Pham et al., "Improving voting feature intervals for spatial prediction of landslides," Mathematical Problems in Engineering, Vol.2020, Article No.4310791, 2020.

[16] T. V. Phong et al., "Landslide susceptibility mapping using Forest by Penalizing Attributes (FPA) algorithm based machine learning approach," Vietnam J. of Earth Sciences, Vol.42, No.3, pp. 237-246, 2020.

[17] B. P. My and N. V. Hoanh (Eds.), "Geological and Mineral Resources Map of Viet Nam on 1:200.000, Kim Binh–Lao Cai zone (F-48-VIII&F-48-XIV)," Department of Geology and Minerals of Vietnam, 2005.

[18] Lao Cai Transport Construction Consultancy Joint Stock Company (LECCO), "Report of technical and geography survey results: The work of upgrading provincial road 152, section Sapa town - Ban Den intersection, belongs to 2nd Mekong Subregion Corridor Urban Development Project (GMS) - Sapa Urban Subproject, Lao Cai city," 2018.

[19] J. Travelletti et al., "Hydrological response of weathered clay-shale slopes: Water infiltration monitoring with time-lapse electrical resistivity tomography," Hydrological Processes, Vol.26, No.14, pp. 2106-2119, 2012.

[20] P. H. Giao and B. X. Hanh, "Analysis of post-landslide electric imaging data at a site in Sapa, Vietnam," Proc. of EAGE-GSM 2nd Asia Pacific Meeting on Near Surface Geoscience and Engineering, pp. 1-5, 2019.

[21] C. F. S. Sharpe, "Landslides and related phenomena," Columbia University Press, 1938.

[22] I. Saunders and A. Young, "Rates of surface processes on slopes, slope retreat and denudation," Earth Surface Processes and Landforms, Vol.8, No.5, pp. 473-501, 1983.

Name:
Manh Duc Nguyen

Affiliation:
Associate Professor, University of Transport and Communications

Address:
No.3 Cau Giay Street, Lang Thuong Ward, Dong Da District, Hanoi, Vietnam

Selected Publications:

• "Features, generation mechanism and urgent treatment solution to the large landslide at Chi Luong resettlement area, Muong Lay Town, Dien Bien Province," Proc. of the 3rd Int. Conf. VIETGEO 2016, pp. 244-251, 2016.

• "Soft-computing techniques for prediction of soils consolidation coefficient," CATENA, Vol.195, Article No.104802, doi: 10.1016/j.catena.2020.104802, 2020.

Name:
Nguyen Van Thang

Affiliation:
Ph.D. Student, Geotechnical Engineering Laboratory, Department of Environmental Engineering Science, Gunma University
Address:
1-5-1 Tenjincho, Kiryu, Gunma 376-8515, Japan

Name:
Akihiko Wakai

Affiliation:
Professor, Gunma University
Address:
1-5-1 Tenjincho, Kiryu, Gunma 376-8515, Japan

Name:
Go Sato

Affiliation:
Professor, Graduate School of Environmental Informations, Teikyo Heisei University
Address:
4-21-2 Nakano, Nakano-ku, Tokyo 164-8530, Japan

Name:
Jessada Karnjana

Affiliation:
National Electronics and Computer Technology Center (NECTEC)
Address:
112 Thailand Science Park, Khlong Luang, Pathum Thani 12120, Thailand

Name:
Hoang Viet Hung

Affiliation:
Associate Professor of Geotechnical Engineering, Thuyloi University
Address:
175 Tay Son Street, Dong Da District, Hanoi, Vietnam

Name:
Lanh Si Ho

Affiliation:
Assistant Professor, Civil and Environmental Engineering Program, Graduate School of Advanced Science and Engineering, Hiroshima University
Lecturer, Faculty of Civil Engineering, University of Transport Technology
Address:
1-4-1 Kagamiyama, Higashihiroshima, Hiroshima 739-8527, Japan

Name:
Indra Prakash

Affiliation:
Former Deputy Director General, Geological Survey of India
Visiting Faculty, Bhaskaracharya National Institute for Space Applications and Geo-Informatics (BISAG)
Address:
Sector 10 A, Gandhinagar, Gujarat 382010, India

Name:
Hoc Tran Quang

Affiliation:
Lecturer, Senior Research Engineer, Faculty of Civil Engineering, University of Transport and Communications
Address:
No.3 Cau Giay Street, Lang Thuong Ward, Dong Da District, Hanoi, Vietnam

Name:
Binh Thai Pham

Affiliation:
University of Transport Technology
Address:
54 Trieu Khuc, Thanh Xuan, Hanoi, Vietnam